

On the development of instability of the black hole-torus systems and quasi periodic oscillations

O. Dönmez^{1*}

¹*Nigde University, Department of Physics, Niğde Turkey, 51200*

Received 2013

ABSTRACT

We present the numerical study of dynamical instability of a pressure-supported relativistic torus, rotating around the black hole with a constant specific angular momentum on a fixed space-time background, in case of perturbation by a matter coming from the outer boundary. Two dimensional general relativistic hydrodynamical equations are solved at equatorial plane using the HRSCS to study the effect of perturbation on the stable systems. We have found that the perturbed torus creates an instability which causes the gas falling into the black hole in a certain dynamical time. All the models indicate an oscillating torus with certain frequency around their instant equilibrium. The dynamic of accreted torus varies with the size of initial stable torus, black hole spin and other variables, such as Mach number, sound speed, initial radius of the torus etc., but not their instability. The precessing torus not only effects the gravitational radiation, but also generates it. On the other hand, the mass accretion rate is slightly proportional to the torus-to-hole mass ratio in the black hole-torus system, but it strongly depends on inner radius of the torus. Increasing the specific angular momentum of the torus outward can lead a more stable torus. Our numerical simulations also show that the oscillating relativistic torus could be used to explain the multiple peaks observed in the black hole high frequency QPOs, responsible for radiation of X-ray observed by different X-ray telescopes.

Key words: general relativistic hydrodynamics: numerical relativity: black hole: torus: instability: quasi-periodic oscillation

1 INTRODUCTION

The coalescing of compact binaries and their interactions with accretion discs are important issues in astrophysics. The recent review about the black hole accretion disc theory given by Abramowicz & Fragile (2013) explains how the interaction of accretion disc with a black hole reveals predictions of emission, signature of strong gravity, black hole mass, and spin. The merging of BH-BH, BH-NS or NS-NS, or accreting a hot matter rotating around compact objects may cause a torus to be formed which might be responsible for oscillation and emission of BH-torus systems. The hot torus around the black hole is thought to be a mechanism gather the particles and form a jet. The internal shocks inside the jets can create high energy particles and lead to the emission of gamma-ray photons (Meszaros 2006). It is important to understand the dynamics, formation, and stability properties of a torus to show how the gamma rays are formed. The rapid destruction of an accretion disc due to high accretion rate, which is larger than the Eddington rate, was first suggested by Abramowicz et al. (1983). They pointed out that the torus, which is rotating in a stable equilibrium around the black hole, might have hydrodynamical

instability owing to non-Keplerian rotation law. The instability of accreting torus orbiting around the non-rotating black hole was studied by Montero et al. (2010), and their numerical simulations showed that axisymmetric oscillation of torus was exhibited without the appearance of the runaway instability. It is also indicated that the self gravity of torus did not play an important role for the occurring of the instability in a few dynamical time steps. The runaway instability was firstly discovered by Abramowicz et al. (1983) using a pseudo-Newtonian potential and studied in relativity by Font & Daigne (2002). Recently, Korobkin et al. (2012), for the first time, demonstrated the runaway instability by using the fully self-consistent general relativistic hydrodynamical evolution. They have confirmed that the runaway instability occurred in a few dynamical times.

The interacting matter with a black hole or falling matter into a black hole is a source of gravitation radiation. Perturbation of the torus by matter modifies the fluid around the black hole and shock may be formed. The rotating shock can cause a matter to have a non-linear behavior and its energy heats the gas. So the electromagnetic flares would be produced and these flayers continue to occur for a long time (Schnittman & Krolik 2008). Interacting particles with shock waves in the equatorial plane produce a continues emis-

* E-mail: odonmez@nigde.edu.tr (OD)

sion ranging from Ultra-Violet to X-rays if they freely drive away from the black hole-torus system.

It is known that the central region of the black hole-disc system, which produces the Gamma Ray Burst (GRB), is not significantly bigger than the size of the black hole. So the torus is a possible physical mechanism to produce GRB and gravitational waves which are used to identify the nature of the inner region that may be observed from GRB system. The small perturbations on the torus create a hydrodynamical instability which is responsible for gravitational waves. Its contribution to the gravitational wave background was estimated by Coward et.al. (2002). The gravitational wave radiation from the center of GRB, which consists of a black hole and torus, was studied by Lee (2004). It was found that the gravitational wave is a natural phenomenon in the wobbling system.

Oscillation properties of the black hole-torus system have been studied for numbers of astrophysical systems. Investigating the oscillating system can allow us to expose discoseismic classes which are dominant in relativistic geometrically thin disc. Some numerical studies revealed the oscillatory modes of the perturbed torus (Zanotti et.al. 2003; Rezzolla et.al. 2003; Montero et.al. 2007). Oscillation properties of the pressure-supported torus were also examined by Schnittman & Rezzolla (2006). They had found a strong correlation between intrinsic frequency of the torus and extrinsic frequency shown in observed light curve power spectrum. The analysis of Quasi-Periodic Oscillations (QPOs) was motivated by observed data coming from the galactic center, low-mass X -ray binaries (van der Klis 2004) and high frequency phenomena, testing the strong gravity (Bursa et.al. 2004) in the innermost region of accretion disc around the black hole.

The Observations with X-ray telescopes have uncovered the existing of QPOs of matter around the black holes (Remillard et.al. 1999; Strohmayer 2001). The QPOs can be used to test the strong gravity and the properties of the black hole since they are originated close to the black hole (Dönmez et.al. 2011; Abramowicz & Fragile 2013). In order to understand these physical properties, the perturbed pressure-supported torus is examined in a close-binary system. In this paper, our main goal is to study the instability of a stable torus on the equatorial plane based on perturbation, which is coming from the outer boundary of computational domain. In order to do that we solve general relativistic hydrodynamical equations in fixed space-time for the non-rotating and rotating black holes at the equatorial plane. Thus, we investigate the effects of perturbation and thermodynamical parameters onto the tori's instability, which causes the appearance of GRBs, in a few dynamical times. We have perturbed the torus in a different way from the one used in Montero et.al. (2007); Schnittman & Rezzolla (2006); Zanotti et.al. (2005); Zanotti & Rezzolla (2003); Font & Daigne (2002) in which it was performed by applying a displacement (or kick) on the torus.

In this work, we study the effect of perturbation onto the torus-black hole system by solving the fully general relativistic hydrodynamical equations in a fixed background. The paper is organized as follows: in section 2, we briefly explain the formulation, numerical setup, boundary and initial condition and introduce the initial setup of relativistic torus. Next, Section 3 describes the numerical results. We present the outcomes of interaction of the torus-black hole system with matter as a result of perturbation coming from the outer boundary. QPOs, due to oscillation of the torus, is also presented. Finally, Section 4 concludes our findings. Throughout the paper,

we use geometrized unit, $G = c = 1$ and space-time signature $(-, +, +, +)$.

2 EQUATIONS, NUMERICAL SETUPS, BOUNDARY AND INITIAL CONDITIONS

2.1 Equations

We consider a spherical symmetric, non-self gravitating a torus with a perfect fluid equation of state in a hydrostatics equilibrium around the non-rotating and rotating black holes. In order to model the instability of the torus due to perturbation, we have solved general relativistic hydrodynamical equations using perfect fluid equation of state. The general relativistic hydrodynamical equations are

$$\nabla_{\mu} T^{\mu\nu} = 0, \quad \nabla_{\mu} J^{\mu} = 0, \quad (1)$$

where $T^{\mu\nu} = \rho h u^{\mu} u^{\nu} + P g^{\mu\nu}$ is a stress-energy tensor for a perfect fluid and $J^{\mu} = \rho u^{\mu}$ is a current density. To preserve and use the conservative properties of general relativistic hydrodynamical equations, Eq.1 is written in a conservative form using the 3 + 1 formalism, and we have (Font et.al. 2000)

$$\frac{\partial \mathbf{U}}{\partial t} + \frac{\partial \mathbf{F}^r}{\partial r} + \frac{\partial \mathbf{F}^{\phi}}{\partial \phi} = \mathbf{S}, \quad (2)$$

where \mathbf{U} is a conserved variable and, \mathbf{F}^r and \mathbf{F}^{ϕ} are fluxes in radial and angular direction at equatorial plane, respectively. These quantities depend on fluid and thermodynamical variables which are written explicitly in detail in Dönmez (2004); Font et.al. (2000). \mathbf{S} represents the source term which depends on space-time metric $g^{\mu\nu}$, Christoffel symbol $\Gamma_{\mu\nu}^{\alpha}$, lapse function α , determinant of three metric γ_{ij} and stress-energy tensor $T^{\mu\nu}$. The conserved variables and fluxes also depend on the velocity of fluid and Lorenz factor. The covariant components of three-velocity v^i can be defined in terms of four-velocity u^{μ} as $v^i = u^i / (\alpha u^t)$ and Lorenz factor $W = \alpha u^0 = (1 - \gamma_{ij} v^i v^j)^{-1/2}$. The explicit representation of general relativistic hydrodynamical equations and their numerical solutions at equatorial plane are given in Dönmez (2004); Yildiran & Dönmez (2010).

2.2 Numerical Setups and Boundary Conditions

We have solved the General Relativistic Hydrodynamics (GRH) equations at the equatorial plane to model the perturbed torus around the black hole. The code used in this paper, which carries out the numerical simulation, was explained in detail by Dönmez (2004), which gives the solutions of the GRH equations using Marquina method with MUSCL left and right states. Marquina method with MUSCL scheme guarantees higher order accuracy and gives better solution at discontinuities mostly seen close to the black hole. The pressure of the gas is computed by using the standard Γ law equation of state for a perfect fluid which defines how the pressure changes with the rest-mass density and internal energy of the gas, $P = (\Gamma - 1)\rho\epsilon$. After setting up the stable torus with a constant specific angular momentum inside the region, $r_{in} < r < r_{max}$, we have to also define the vacuum, the region outside of the $r_{in} < r < r_{max}$ at where all the variables set to some negligible values. We have used dynamically unimportant numbers for atmosphere, $\rho_{atm} = 10^{-12}$. The Kerr coordinate is used to set up the black hole at the center of computational domain

using an uniformly spaced grid in r and ϕ directions. The r goes from $2.8M$ to $200M$ for non-rotating, and $1.7M$ to $200M$ for rotating black holes while ϕ varies between 0 and 2π . Typically, we use $N_r \times N_\phi = 3072 \times 256$ zones in radial and angular directions at the equatorial plane.

The boundaries must have been correctly resolved to avoid unwanted oscillations. So we set up an outflow boundary condition at physical boundaries of computation domain in radial direction. All the variables are filled with values using zeroth-order extrapolation. While the velocity of matter, v^r , must be less than zero at close to the black hole, it should be bigger than zero at the outer boundary of computation domain. The periodic boundary condition is used in angular direction.

2.3 Initial Torus Dynamics

The analytic representation of the non-self-gravitating relativistic torus for a test particle was first examined by Abramowicz et.al. (1978). They found a sharp cusp for marginally stable accreting disc which was located at an equatorial plane. Later, torus with a perfect fluid equation of state was discussed in detail in Refs. Zanotti & Rezzolla (2003); Zanotti et.al. (2003, 2005); Nagar et.al. (2005), numerically. The matter of torus is rotating at a circular orbit with non-geodesic flow between r_{in} and r_{max} , and the polytropic equation of state, $P = K\rho^\Gamma$, is used to build an initial torus in hydrodynamical equilibrium with the values of variables given in Table 1. Using the $\Gamma = 4/3$, it mimics a degenerate relativistic electron gas. The significant internal pressure in torus can balance the centrifugal and gravitational forces to maintain the system in hydrodynamical equilibrium.

Almost all the astrophysical systems, which have a torus type structure, are expected to form as a consequence of the merger of two black holes, two neutron stars, their mixed combination or form in the core collapse of the massive stars. These phenomena suggest that the torus might be in non-equilibrium state after it is formed. In order to understand the physical phenomena of a non-stable black hole torus system and perturbation of the torus by a matter which is coming from outer boundary of computational domain, we have considered different initial conditions and perturbations given in Table 1.

3 NUMERICAL RESULTS

The numerical results given in this paper are classified depending on the torus-to-black hole mass ratio and black hole spin as well as the size of the pressure-supported stable torus around the black hole. The perturbing torus will uncover its oscillating properties of and dynamical exchange during the evolution.

We adopt the perturbation from the outer boundary at $3.1 < \phi < 3.18$ with parameters, sound speed, and Mach number given in Table 1 and rest-mass density of perturbation is $\rho_p = \rho_c - 0.1\rho_c$ for all models. The matter is injected toward the torus-black hole system with radial velocities, $V^r = 0.002$, $V^r = 0.02$, $V^r = 0.2$, and $V^r = 0.0001$ and with angular velocity, $V^\phi = 0.00001$ for all V^r , accelerated radially and reached the torus around $t = 3000M$. We apply the perturbation inside the region where gravitational forces are dominant, almost causing the matter to fall toward the black hole radially. The period of matter at the center of torus is around $T_c = 170M$. The perturbation starts to influence the torus after ~ 16 orbital period of the torus which has highest density around $r \approx 9M$. But it is ~ 4 orbital period for models P_1 and P_2 given

in Table 1. These orbital periods are measured at the location of the rest-mass density maximum in the unperturbed torus.

3.1 Perturbed Torus Around the Non-Rotating Black Hole

The perturbations sent into the black hole-torus system trigger the matter falling into the black hole due to the instability causing the sudden X-ray flare. The observed X - rays which hit the local gas of torus produce light echo. Because the torus around the non-rotating and rotating black holes may shrink and come closer to the black holes. Hence, it constitutes more hot region to generate higher X-ray fluxes.

To analyze the dynamics of the torus and its instability after the perturbation, we plot the density of the torus for the inner region at different snapshots for model P_1 seen in Fig.1. The torus, initially stable, is perturbed by matter coming from the outer boundary. In the color scheme while the red is representing the highest density, the blue shows the lowest value of the torus's density. At $t \sim 3000M$, perturbation hits the pressure-supported stable torus and then the spiral structure with a steady state case is developed as time progress. Once the perturbed torus reaches the steady state, the non-axisymmetric dynamical features are introduced in the accreted torus. This steady state structure rotates around the black hole and produces quasi-periodic oscillation. The inner radius of torus gets more closer to the black hole. The rotating gas represents wave-like behavior and it travels inward or outward. From Fig.1, we conclude that the torus stays in steady state and the inner radius is located around $r = 15M$ before it interacts with perturbation. After the perturbation, the inner radius of the torus gets closer to the black hole. As a result the location of cusp of the perturbed torus moves toward to black hole and the accreted torus reaches to a new equilibrium state. After all the distribution of density is almost spherically symmetric. It is also seen in the color plots that the perturbed torus has oscillatory behavior, and the oscillation amplitude stays almost constant during the compression and expansion of the torus.

The rotating torus has centrifugal forces which pull out gas outwardly around the black and causes less the gas accret than the Bondi rate during the perturbation. The angular velocity of the torus is larger than Keplerian one, and it exponentially decays for the larger r . The distribution of angular momentum is maintained by the disc pressure. The angular momentum of the torus close to the horizon may be transferred to the black hole after the torus is perturbed. This transformation can be used to explain the spin up of the black hole.

In order to reveal the effect of the size of torus and inner radius onto the instability and dynamics of the torus, we consider the perturbations of the tori for the same mass, but with different sizes. The time evolution of the central rest-mass density of torus, each of them plotted along r at $\phi = 0$, are shown for models P_1 and P_3 in Fig.2. For these models, we have applied a perturbation, which is $\rho_p = \rho_c - 0.1\rho_c$, from the outer boundary between $t = 0M$ and $t = 80M$ to evolve the influence of perturbation to the overall dynamics of torus. The perturbation destroys the torus, triggers the instability and can cause the location which has the maximum density to approach the horizon. Such perturbation induces the matter to fall into the black hole or out from computational domain. While the maximum rest-mass density of torus slightly oscillates for model P_1 , seen in the right panel of Fig.2, the rest-mass density significantly decreases, seen in the left panel of the same graph, during the time evolution.

Accretion rate shows time variation in a great amplitude

Table 1. Initial models of the perturbed torus around the black hole at the equatorial plane. From left to right: P shows the model name, a is the spin parameter of the black hole, M_t/M_{BH} is the torus-to-hole mass ratio, Γ is the adiabatic index, $K(geo)$ is the polytropic constant in geometrized unit, ℓ_0 is the constant specific angular momentum, $r_{cusp}(M)$ is the cusp location, $\rho_c(geo)$ is the density at the center of the torus, r_c and $r_{in}(M)$ are the inner radii of the last stable orbit and location at where density is maximum, C_s and \mathcal{M} are the speed of sound and the Mach number of perturbation, respectively. *Perturbation* shows the type of perturbation applied on the torus. The total time of the simulations varies depending on models.

Model	$\frac{a}{M}$	$\frac{M_t}{M_{BH}}$	Γ	$K(geo)$	$\rho_c(geo)$	ℓ_0	$r_{cusp}(M)$	$r_{in} - r_c(M)$	Parameters		Injected Matter <i>Perturbation</i>
									$C_s(c)$	of \mathcal{M}	
P_1	0.0	0.1	4/3	4.969×10^{-2}	7.329×10^{-5}	5.44	2.91	15 – 25	0.001	2	$t \rightarrow 0 - 80M$
P_2	0.0	0.1	4/3	4.969×10^{-2}	7.329×10^{-5}	5.44	2.91	15 – 25	0.001	2	<i>continues</i>
P_3	0.0	0.1	4/3	4.969×10^{-2}	1.140×10^{-4}	3.80	4.57	4.57 – 8.35	0.001	2	$t \rightarrow 0 - 80M$
P_4	0.0	0.1	4/3	4.969×10^{-2}	1.140×10^{-4}	3.80	4.57	4.57 – 8.35	0.01	2	$t \rightarrow 0 - 80M$
P_5	0.0	0.01	4/3	3.184×10^{-2}	2.863×10^{-6}	3.95	4.107	5.49 – 9.97	0.001	2	$t \rightarrow 0 - 80M$
P_6	0.0	1	4/3	2.294×10^{-2}	1.153×10^{-3}	3.80	4.57	4.57 – 8.35	0.001	2	$t \rightarrow 0 - 80M$
P_7	0.0	0.1	4/3	3.601×10^{-2}	1.628×10^{-4}	3.784	4.64	4.64 – 8.16	0.001	2	$t \rightarrow 0 - 80M$
P_8	0.0	1	4/3	2.294×10^{-2}	1.153×10^{-3}	3.80	4.57	4.57 – 8.35	0.001	200	$t \rightarrow 0 - 80M$
P_9	0.0	0.1	4/3	3.601×10^{-2}	1.628×10^{-4}	3.784	4.64	4.64 – 8.16	0.001	0.1	$t \rightarrow 0 - 80M$
P_{10}	0.9	0.1	4/3	4.969×10^{-2}	1.140×10^{-4}	2.60	1.78	1.78 – 3.40	--	--	--
P_{11}	0.9	0.1	4/3	4.969×10^{-2}	1.140×10^{-4}	2.60	1.78	1.78 – 3.40	0.001	2	$t \rightarrow 0 - 80M$
P_{12}	0.9	0.05	4/3	4.969×10^{-2}	1.999×10^{-5}	3.303	1.41	5.78 – 7.40	0.001	2	$t \rightarrow 0 - 80M$

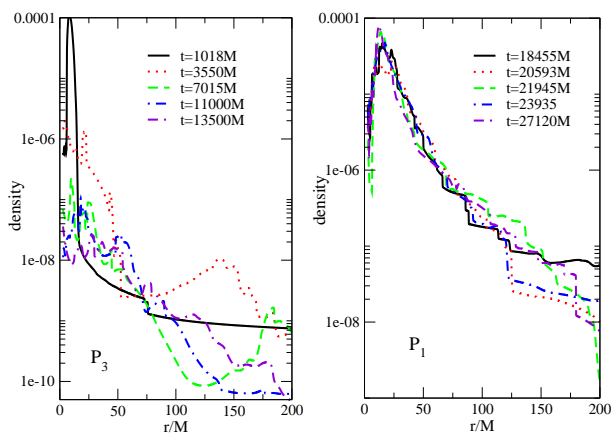


Figure 2. Time evolution of rest-mass density along the r for model P_3 (left panel) and model P_1 (right panel).

similar to one happening in low or hard X-ray time variation. Computing the accreting and the mass accretion rate are important indicators to understand the disc behavior and its instability around black holes. Instability of accreted torus can be subject to perturbation coming from the outer boundary in a number of circumstances which may cause unstable mass accretion rates (Papaloizou & Pringle 1984, 1985). We have confirmed that the accretion rate is governed by some physical parameters: torus-to-hole mass ratio, the location of inner radius, initial specific angular momentum of the torus, Mach number of the perturbed matter and the angular momentum of the black hole. The mass accretion rate computed from P_1 , P_3 , and P_4 are depicted in the left part of Fig.3. We have noticed that the mass accretion rate for the models are the same at early times of simulations, but later the models, P_3 and P_4 , drop exponentially as a function of time. Interestingly, the mass accretion rate for only model P_1 does not increase in amplitude, and it oscillates around $dM/dt = 5 \times 10^{-5}$.

The mass accretion rate of the perturbed torus produces luminosity associated with the central engine of gamma ray burst. The expected maximum accretion rate from the gamma ray burst is as high as $dM/dt \approx 0.01 - 1M_\odot/s$ (Chen & Beloborodov 2007). Fig.3 indicates that the computed mass accretion rate from

our numerical simulations, $\frac{dM}{dt} \sim 2 \times 10^5 (\frac{M_\odot}{s}) \frac{dM}{dt}(geo)$ where $\frac{dM}{dt}(geo)$ is the mass accretion rate in geometrized unit, is in order of or slightly higher than the expected maximum accretion rate. It is also shown in the left panel of Fig.3 that the mass accretion rate suddenly increases after perturbation reaches to the torus and shortly after the Papaloizou-Pringle instability is developed. It reaches its maximum value and oscillates around a nonzero constant value.

It is obvious from the right part of Fig.3 that the accretion rates exponentially decay during the time and is always bigger when the mass ratio of the torus-to-black hole is larger. Decaying a mass accretion rate reaches a constant value $dM/dt \approx 0.1M_\odot/s$ around $t = 14000M$ ($t = 82t_{orb}$). It is in good agreement with the expected accretion rates for accreting disc with the GRBs. As it can be seen in Fig.3, the amplitude of mass accretion rate and its behavior manifest a dependence on the mass ratio of the torus-to-black hole and inner radius of the torus. While the mass accretion rates for all models decay with time due to the strong gravity which overcomes angular momentum of the torus, it oscillates around a certain rate for model P_1 , shown in Fig.3. The oscillatory behaviors of all models are seen obviously during the time evolution. When the accreted torus gets close to the black hole, the mass accretion rate and instability of the torus depend on the inner radius of the torus and the spin of the black hole.

The continuous perturbation of the black hole-torus system can lead not only instability of the torus but also oscillates of its dynamics around the certain points, seen in Fig.4. The left panel in Fig.4 exhibits the time variation of mass accretion rate for model P_4 computed for $r = 8M$ which is true for the perturbed matter injecting from the outer boundary continuously. It is seen in this plot that the perturbation starts to interact with a torus around $t \sim 3000M$, and then nonlinear oscillation is developed. It is noted that the continuous perturbation can create different types of dynamical structures and accretion rates.

The higher specific angular momentum of the torus outwards can allow the torus to become more stable. Fig.5 shows the specific angular momentum of the torus along the radial coordinate for models P_1 , P_3 , P_6 , and P_7 . It becomes apparent that the increasing of the specific angular momentum outwards leads to stabilize the torus and suppresses the runaway instability. It is also confirmed by Figs.1 and 3.

Fig.6 represents the time evolution of the maximum rest-mass density at the center of the torus, each of them normalized to their

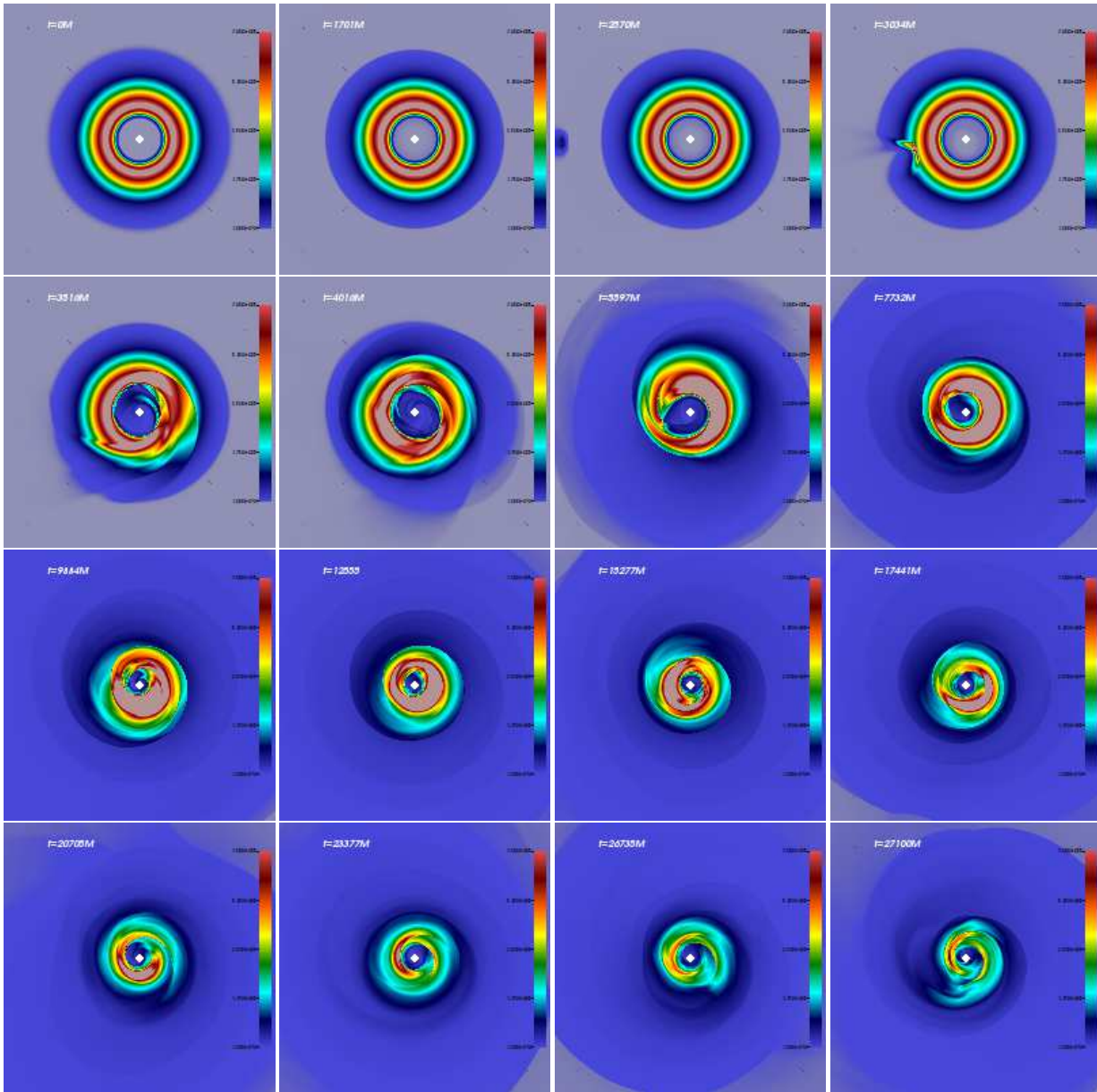


Figure 1. The rest-mass density of perturbed torus during the time evolution for Model P_1 . The torus is perturbed by a matter coming from outer boundary. The matter interacts with the torus around $t = 3034M$ and distorts it. The instability is formed at $t = 4540M$ and stays during the evolution. The structure of the torus is highly turbulent and makes quasi-periodic oscillation.

initial values, for models P_5 , P_6 , P_7 , P_8 , and P_9 . For these models, we have applied the same perturbation with different densities ($\rho_p = \rho_c - 0.1\rho_c$), giving the first kick to the black hole-torus system. The matter begins to influence the torus around $t = 3120M$. The perturbation triggers the non-stable oscillation of the torus for models given in Fig.6 except the model P_8 . These models exponentially decay and produce sharp peaks after perturbation reaches the torus. Thus, these results imply that subsonic or mildly supersonic perturbation produces the pressure-supported oscillating torus around the black hole, and amplitude of the oscillation gradually decreases while the Mach number of perturbation increases. Such oscillations can cause the matter to fall into the black hole or outward from the computational domain. These physical phenomena can significantly reduce the rest-mass density of the torus during the time evolution seen in Fig.6. Depending on the initial

configurations, such as, mass ratio of the torus-to-hole and inner radius of the last stable orbit of the torus, the reducing rate of rest-mass density is defined at the end of simulation. The density of the stable initial torus having an initial radius $r_{in} = 5.49M$ given in model P_5 decreases slower than the one with the smaller inner radius given in models P_6 , P_7 , P_8 , and P_9 . This result is also confirmed by model P_1 . The matter of the torus close to the black hole would fall into the black hole due to the strong gravity after the torus is triggered by perturbation. Therefore, the mass of the black hole and its spin would increase with time significantly. We also note that the reduction of the rest-mass density for model P_6 is slightly slower than the model P_7 . So the lower the torus-to-hole mass ratio loses the faster the matter during the evolution. But it needs a further consideration to reveal a global conclusion.

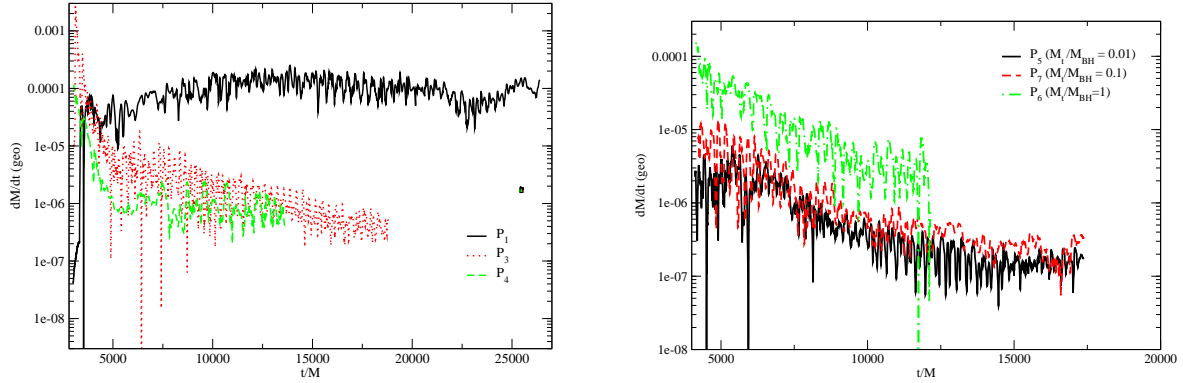


Figure 3. Left panel: the mass accretion rates for models P_1 , P_3 , and P_4 computed at $r = 6M$ in geometrized unit. Three different models, the torus with different $r_{in} - r_c$ while keeping the same sound velocity or vice versa, are considered to show the effect of perturbation on the torus. Right panel: mass accretion rate for models P_5 , P_6 , and P_7 .

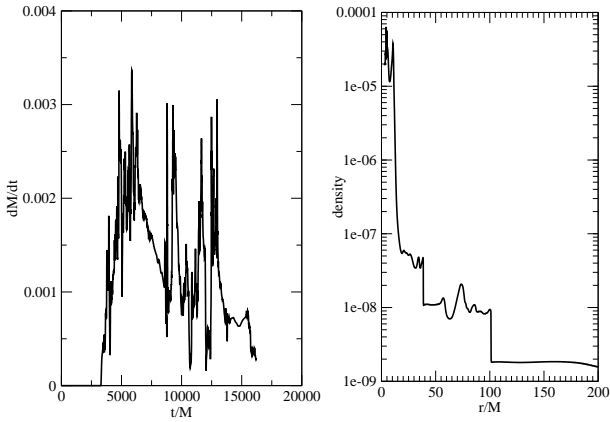


Figure 4. The mass accretion rate (left panel) and the rest-mass density of torus along r (right panel) are plotted for model P_2 .

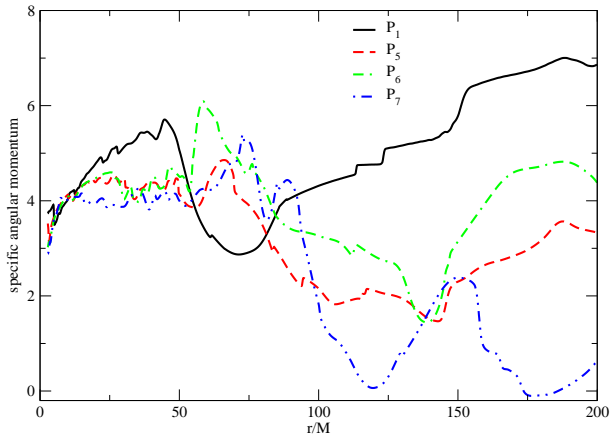


Figure 5. The specific angular momentum for models P_1 , P_5 , P_6 , and P_7 is plotted as a function of radial coordinate a long time later that the disc is perturbed and instability is developed.

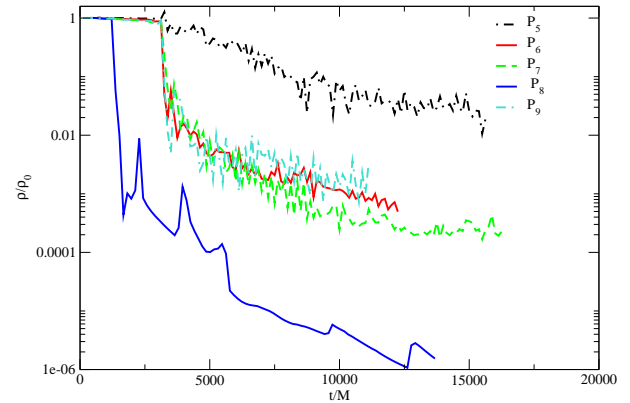


Figure 6. The variation of the maximum density of torus in logarithmic scale as a function of time, each of them normalized to its initial value $\rho_0 \equiv \rho_c$, for the models, P_5 , P_6 , P_7 , P_8 , and P_9 . The torus loses the matter during the time evolution for all cases while it is almost stable before the perturbed matter reaches the torus.

3.2 Perturbed Torus Around the Rotating Black Hole

In order to put forth the effect of the rotating black hole onto the perturbed torus, we have perturbed the stable torus orbiting around the rotating black hole using the initial parameters given in models, P_{10} , P_{11} , and P_{12} in Table 1. We have analyzed the time evolution of the rest-mass density of the torus with/without perturbation and found that perturbed tori given in models, P_{11} and P_{12} , become unstable before the perturbation reaches to them but the structure of unperturbed torus never changes during the evolution shown in Fig.7. We note that the results of perturbation effect from the non-rotating black hole contradicts to the results obtained from rotating case.

The perturbations on the tori having different inner radii and total mass produce diverse dynamics. The small perturbation onto the high mass torus, which is more closer to the black hole, induces the stable torus before the perturbation reaches to it. The spiral pattern is produced around the rotating black hole, and it causes the gas falling into the black hole during the simulations. At the same time, it also creates regular oscillation seen in the second and third rows of Fig.7 and model P_{11} in Fig.8. It is obvious from the

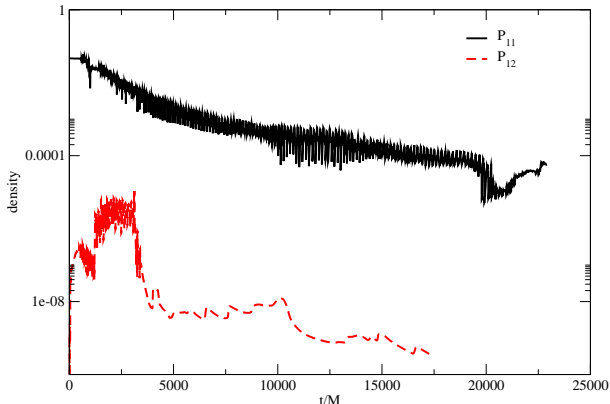


Figure 8. The time evolution of rest-mass density at a fixed point on the torus for models, P_{11} and P_{12} , for $a = 0.9$. The inner radii of the models are different, but the same perturbation is applied to the both models.

model P_{12} in Fig.8 and, last two rows of Fig.7 that the torus responds somewhat differently to the applied perturbation, and the torus with a low mass, which is far away from the black hole, has a non-oscillatory behavior. Both of these models indicate that at the end of the simulation, the rest-mass density of the torus is reduced substantially. On the other hand, it is shown that the perturbed torus, which has a cusp located inside the black hole, has a non-linear dynamic during the evolution as seen in the last two rows of Fig.7.

3.3 QPOs from the oscillating Torus

We have performed the simulations using different values of r_{in} and r_c of the initial torus with a perturbation given in Table 1. For these initial perturbed discs, the global oscillations are seen at various frequencies. Perturbations to a perfectly stable torus give rise to an epicyclic motion in radial direction due to the oscillation mode. Fig.9 consists of a fundamental frequency at $\sim 199Hz$ and number of overtones, $\sim 399Hz$, $\sim 600Hz$, $\sim 800Hz$ etc. that they can determine the ratios 1:2:3:.... It suggests that the non-linear oscillation of the torus due to the perturbation is a consequence of fundamental modes of the torus. The power law distribution given in the right panel of Fig. 9 indicates how the peaks appear as a function of ϕ at fixed $r = 8.12M$ which almost represents the point of maximum density of the torus. The amplitudes for the corresponding peaks are almost the same for all ϕ at the same frequencies. In both graphs, two strong narrow peaks occur at $\sim 199Hz$ and $\sim 399Hz$. The QPO behavior of the oscillating torus found in our work might be used to explain commensurability frequencies observed in the sources, *H1743322*, *XTE J1550564*, and *GRS 1915 + 105* (McClintock & Remillard 2004).

The QPO's frequencies from our simulation for the black hole $M = 2.5 M_{\odot}$ are approximately the same as found in Zanotti & Rezzolla (2003); Zanotti et.al. (2003). They computed the power spectrum of the L_2 norm error of the rest-mass density for different η after the long time evolution. The fundamental frequencies, which are seen around $200Hz$, and the series of overtones for both cases are observed. Our study indicates that the perturbed torus, which is caused either by the introduction of a suitable parametrized perturbation to the radial velocity Zanotti & Rezzolla (2003); Zanotti et.al. (2003) or by a matter coming toward the torus, may produce regular oscillatory behavior. The modes observed

from both perturbations are called the pressure (p) mode of oscillation of the torus. The small size of accretion torus orbiting around the black hole can be used to explain p mode in high frequency quasi-periodic oscillations (Abramowicz & Kluzniak 2004). The p mode represents the oscillation of matter in the horizontal direction at the equatorial plane and is trapped inside the torus. Due to the two-dimensional structure of the system, the magnetic field did not create a strong effect on the wave properties of p mode (Fu & Lai 2009).

It is known from previous discussion that the torus loses matter during time evolution, and it has chaotic behavior seen in models P_3 and P_4 . Due to this irregular non-linear oscillation, only a fundamental mode appears, but their overtones are absent in the power spectrum when the torus is initially more close to the black hole. We suggest that the variation of the torus's matter results from the non-spherical symmetric perturbation of the inner accreted torus.

We have also analyzed the time evolution of mass accretion rate for the model, P_{11} reported in Table 1 to compute Fourier spectra of the perturbed torus around the rotating black hole. After the perturbation starts to influence the torus dynamics, mass accretion rate oscillates around its equilibrium point. Due to a distinctive quasi-periodic oscillation of the unstable torus, the periodic character of the spiral structure becomes more evident after perturbation reaches to the torus a long time later. After the torus relaxes to regular oscillation, it loses the mass, and the oscillation amplitude decreases during the evolution. The computing QPO frequencies from the mass accretion rate might not give definite information, but we may approximately predict it. The power spectra of mass accretion rate shows a fundamental mode with a strong amplitude at $500Hz$ and series of overtones located at $1001Hz$, $1491Hz$, and $1998Hz$ for $a = 0.9$ and $M = 2.5 M_{\odot}$. It is worth emphasizing that a fundamental frequency from the torus around the rotating black hole is much larger than the non-rotating case seen in Table 2. This is an acceptable result because the torus is more closer, and gravity is more stronger in case of the rotating black hole. Table 2 also suggests that a linear scaling is present for the black hole spin.

The observed high frequency QPOs around the black holes and neutron stars were described by Kluzniak & Abramowicz (2001); Abramowicz & Kluzniak (2001); Blaes et.al. (2007); Mukhopadhyay (2009); Mukhopadhyay et.al. (2012) using a single model which has addressed the variation of QPO frequencies. Based on the proposed model, they had predicted the spin of the black hole using the observed QPO pairs which seem to appear at a 3 : 2 ratio. The lower and higher frequencies of pairs for any system are $\nu_l = \nu_{\perp} - \nu_s/2$ and $\nu_h = \nu_r + \nu_s$, respectively. Here, ν_{\perp} , ν_r and ν_s are theoretical values of radial, vertical epicyclic frequencies (Dönmez 2007) and spin frequency of the black hole, respectively. Using the above model we find that the computed commensurable frequency, 600 : 399, is exposed at $\sim 8.1M$. The estimated value of location of resonance from numerical computation, which is $\sim 9M$, is in the suitable range of theoretical calculation.

4 CONCLUSION

We have performed the numerical simulation of the perturbed accreted torus around the black hole and uncovered the oscillation properties to compute QPOs. Instead of giving any kick to a stable torus studied by different authors in literature, the matter is sent from the outer boundary toward the torus-black hole system to perturb it. We have initially considered the different sizes of the stable tori and torus-to-hole mass ratios to expose oscillations of the tori,

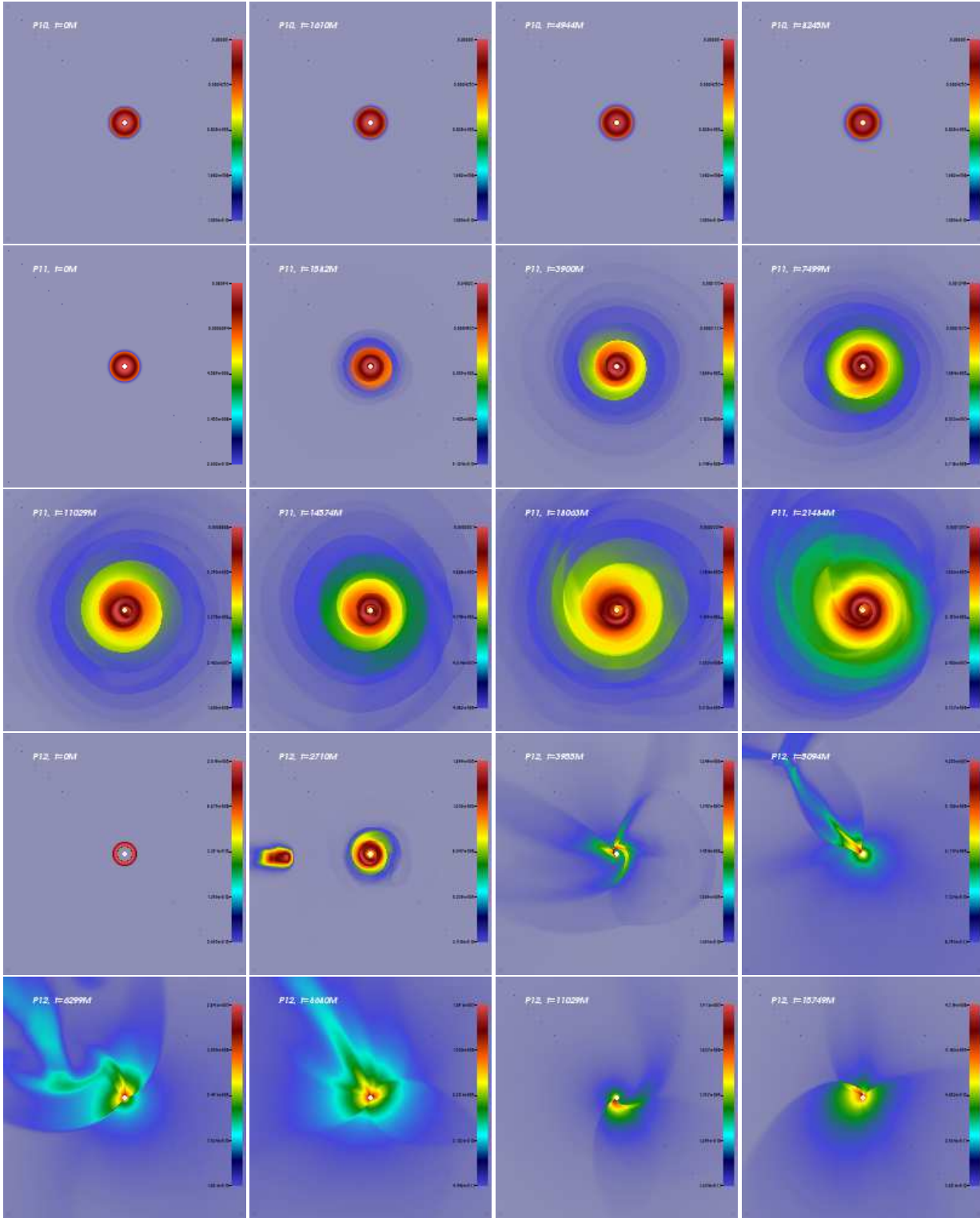


Figure 7. Density ρ of the torus at the equatorial plane for different models, P_{10} , P_{11} , and P_{12} with a black hole rotation parameter, $a = 0.9$. While the top row shows the unperturbed torus around the rotating black hole, the others indicate the perturbation of torus having different size and density.

and computed the fundamental modes and their overtones which results from the excitation of frequencies due to perturbation.

We have confirmed that the torus around the black hole might have quasi-periodic oscillation only if we choose a suitable initial data for stable accretion torus. There are a number of different

physical parameters which may affect the oscillation properties of the torus. It is seen from our numerical simulations that the size of torus affects the frequencies of oscillating torus and their overtones. The size of torus and its rest-mass density also influence the power of oscillations and this oscillation creates radiation of hotter

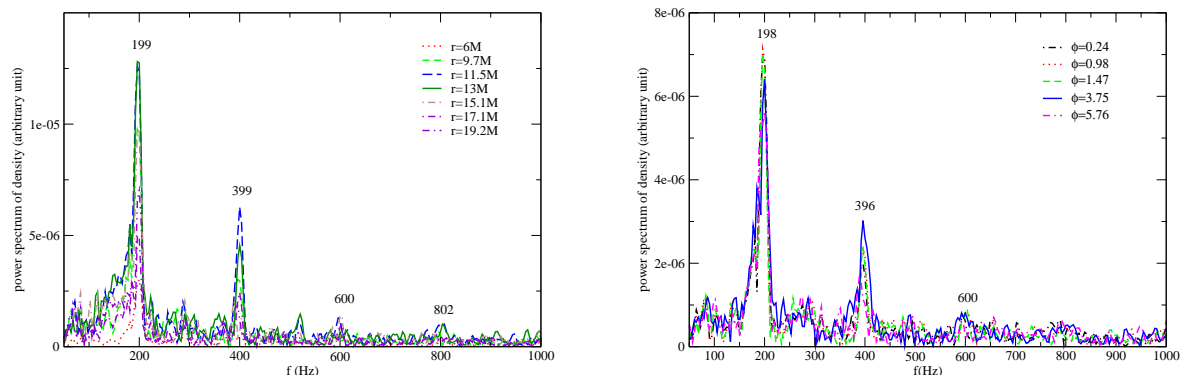


Figure 9. Power spectrum of the rest-mass density at a single point (any ϕ or r) for $M = 2.5 M_{\odot}$ for model P_1 shown in Table 1. A fundamental frequency appears at far left of the both graphs. The others are the consequence of overtones.

Table 2. The frequencies of genuine mode and its series of overtones, due to the nonlinear coupling, inside the torus from the evolution of mass accretion rate. It is computed for different black hole spins while the mass of the black hole is assumed to be $M = 2.5 M_{\odot}$.

Model	a/M	$f_1 [Hz]$	$o_1 [Hz]$	$o_2 [Hz]$	$o_3 [Hz]$
P_1	0.0	199	399	600	800
P_{11}	0.9	500	1001	1491	1998

photons. The similar conclusion has been also confirmed by Bursa (2005). The oscillation and mass losing rate of the perturbed torus strongly depend on the Mach number of perturbing matter. Upon the given appropriate parameters of perturbation, the subsonic or mildly supersonic flow produces the pressure-supported oscillating torus around the black hole and the amplitude of oscillation gradually decreases while the Mach number of perturbation increases. We have found that the rest-mass density of torus substantially decreases during the evolution in most of the models given in Table 1. The disc would entirely fall into the black hole, and the mass of the black hole would grow.

Our studies also indicate that QPOs are common phenomena on the disc around the black holes. If the accretion disc or torus have quasi-periodic behavior, it emits continuous radiation during the computation. The amplitude of oscillation is excited by nonlinear physical phenomena. It has been explained in terms of the excitation of pressure gradients on the torus and it is called p mode. It is shown that the power law distribution of oscillating stable torus includes a fundamental frequency at $\sim 199Hz$ and their number of overtones, $\sim 399Hz$, $\sim 600Hz$, and $\sim 800Hz$ that they can determine the ratios $1 : 2 : 3 : 4$. These frequencies are observed at any radial and angular directions of the torus. The computed QPO frequencies are almost the same as found by Zanotti & Rezzolla (2003); Zanotti et.al. (2003) even though they apply a kick to the radial velocity of the torus in order to have an oscillation. We have also confirmed that the fundamental QPO frequencies and their overtones for rotating black hole are much higher than the non-rotating case due to strong gravity and location of the inner radius of the accreted torus. The strong gravity plays a dominant role in the high frequency modulation of observed X-ray flux in the binary system (Bursa et.al. 2004). It is consistent with the computation from our simulations seen in Table 2.

We have also reported that the initial perturbation induces the torus-black hole system to start the instability around the rotating black hole before the transferred matter reaches to the black hole.

The perturbation can also lead the matter of the torus to fall into the black hole. It reduces significantly the total rest-mass density of the torus with time, and the oscillatory behavior of the rest-mass density changes depending on the inner radius of the torus.

Finally, we have performed the numerical simulation using $2D$ code on the equatorial plane. Clearly, to investigate the effects of forces in the vertical direction on torus instability that may play an important role on the dynamics of the whole system, $3D$ numerical simulations are required. The mode coupling in the vertical direction is likely to affect the instability of a perturbed torus-black hole system. Therefore, we plan to model the same perturbed system by using $3D$ code in the future.

ACKNOWLEDGMENTS

We would like to thank the anonymous referee for constructive comments on the original version of the manuscript. The numerical calculations were performed at the National Center for High Performance Computing of Turkey (UYBHM) under grant number 10022007.

REFERENCES

- Abramowicz, M. A. & Fragile, P. C. 2013, Living Rev. Relativity, 16, arXiv:1104.5499.
- Abramowicz, M. A., Jaroszynski, M. & Sikora, M. 1978, A&A, 63, 221-224.
- Abramowicz, M. A., & Kluzniak, W. 2001, A&A, 374, L19-L20.
- Abramowicz, M. A., Calvani, M. & Nobili, L. 1983, Nature, 302, 597-599.
- Abramowicz, M. A. & Kluzniak, W. 2004, X-Ray Timing 2003: Rossi and Beyond, astro-ph/0312396
- Blaes, O. M., Sramkova, E., Abramowicz, M. A., Kluzniak, W. & Torkelsson, U. 2007, ApJ, 665, 642-653.

- Bursa, M. 2005, *Astron.Nachr.* 326, 849-855.
- Bursa, M., Abramowicz, M. A., Karas, V. & Kluzniak, W. 2004, *ApJ*, 617, L45-L48.
- Chen, W. & Beloborodov, A. M. 2007, *ApJ*, 657, 383.
- Coward, D. M., van Putten, M. H. P. M., & Burman, R., R. 2002, *ApJ*, 580, 1024.
- Dönmez O. 2004, *Astrophys. Spac. Sci.*, 293, 323.
- Dönmez O., Zanotti, O., & Rezzolla, L. 2011, *MNRAS*, 412, 1659.
- Donmez O. 2007, *MPLA*, 22, 141-157.
- Font, J. A. & Daigne, F. 2002, *MNRAS*, 334, 383.
- Font, J.A., Miller, M., Suen, W.-M. & Tobias, M. 2000, *Phys. Rev. D*, 61, 044011.
- Kluzniak, W. & Abramowicz, M. A. 2001, *astro-ph/0105057*.
- Korobkin, O., Abdikamalov, E., Stergioulas, N., Schnetter, E., Zink, B., Rosswog, S. & Ott, C. 2012, *astro-ph/arXiv:1210.1214*.
- Lee, H., K. 2004, *Journal of Korean Physical Society*, 45, 1746.
- Fu, W. & Lai, D. 2009, *ApJ*, 690, 1386.
- McClintock J. E. & Remillard R. 2004, in Lewin W. H. G., van der Klis M., eds, *Compact Stellar X-Ray Sources*. Cambridge University Press, Cambridge.
- Meszaros, P. 2006, *Rep. Prog. Phys.*, 69, 2259.
- Montero, P. J., Zanotti, O., Font, J. A. & Rezzolla, L. 2007, *MNRAS*, 378, 1101.
- Montero, P. J., Font, J. A. & Shibata, M. 2010, *PRL*, 104, 191101.
- Mukhopadhyay, B. 2009, *ApJ*, 694, 387-395.
- Mukhopadhyay, B., Bhattacharya, D. & Sreekumar, P. 2012, *IJMPD*, 21, 1250086.
- Nagar, A., Font, J. A., Zanotti, O. & de Pietri, R. 2005, *PRD*, 72, 024007.
- Remillard, R. A., Morgan, E. H., McClintock, J. E., Bailyn, C. D. & Orosz, J. A. 1999, *ApJ*, 522, 397-412.
- Rezzolla L, Yoshida S and Zanotti O 2003a, *MNRAS*, 344, 978.
- Papaloizou, J. C. M. & Pringle, J. E. 1984, *MNRAS*, 208 721.
- Papaloizou, J. C. M. & Pringle, J. E. 1985, *MNRAS*, 213 799.
- Schnittman, J & Rezzolla, L. 2006, *ApJ*, 637L, 113S.
- Schnittman, J. D. & Krolik, J. H. 2008, 684, 835.
- Strohmayer, T. E. 2001, *ApJ*, 552, L49.
- van der Klis M 2004, eprint *arXiv:astro-ph/0410551*.
- Zanotti, O., Font, J. A., Rezzolla, L. & Montero, P. J. 2005, *MNRAS*, 356, 1371.
- Yildiran, D. & Dönmez O. 2010, *IJMPD*, 19, 2111-2133.
- Zanotti, O & Rezzolla, L. 2003 *MSAIS*, 1, 192.
- Zanotti O, Rezzolla L and Font J A 2003, *MNRAS*, 341, 832.